Excitation Functions and Nuclear Charge Dispersion in the Fission of Uranium by 0.1- to 6.2-GeV Protons*

G. FRIEDLANDER, L. FRIEDMAN, B. GORDON,† AND L. YAFFE‡
Chemistry Department, Brookhaven National Laboratory, Upton, New York
(Received 27 September 1962)

Cross sections for formation of cesium and rubidium isotopes produced by bombardment of uranium with protons ranging in energy from 0.1 to 6.2 GeV were measured both radiochemically and mass spectrometrically. Independent yields were determined for Rb^{84}, Rb^{86}, Cs^{127}, Cs^{129}, Cs^{130}, Cs^{131}, Cs^{132}, Cs^{134}, Cs^{136}, and, at some energies, Rb^{83} and Cs^{135}. In addition, the independent yield of Ba^{131} and the chain yields of Cs^{125}, Cs^{127}, Cs^{129}, La^{131}, Cs^{135}, Cs^{137}, Rb^{83}, Rb^{87}, and Ba^{140} were obtained. The formation cross sections of the Cs and Ba products on the neutron-excess side of stability decrease monotonically with increasing energy above 0.1 GeV, whereas the excitation functions for independent formation of the more neutron-deficient products in the Cs-Ba region and of Rb^{84} and Rb^{86} all go through maxima. The proton energies at which these maxima occur fall on a smooth curve when plotted against the neutron-proton ratio of the product, with the peaks moving to higher energies with decreasing neutron-proton ratio. Under the assumption that the mass-yield curve in the region $125<A<140$ is rather flat at each proton energy, the cross-section data in the Cs region can be used to deduce the charge dispersion in this mass range. Plots of $\log\sigma$ vs N/Z (or $Z-Z_A$) show symmetrical bell-shaped peaks up to a bombarding energy of 0.38 GeV, with full width at half-maximum increasing from 3.3 Z units at 0.10 GeV to about 5 Z units at 0.38 GeV, and with the peak position (Z_p) moving from $Z_A-1.44$ to $Z_A-0.85$ over the same energy range. At all higher energies, a double-peaked charge distribution was found, with a neutron-excess peak centered at $N/Z\sim1.515(Z_p\sim Z_A-1.9)$, and having approximately constant width and height at bombarding energies greater than 1 GeV. The peak on the neutron-deficient side which first becomes noticeable at 0.68 GeV appears to become broader and shift slightly to smaller N/Z values with increasing energy. The two peaks are of comparable height in the GeV region, and the peak-to-valley ratio is only ~2. The total formation cross section per mass number in the Cs region decreases from ~52 mb at 0.1 GeV to about 29 mb at 1 GeV and then stays approximately constant; the contribution of the neutron-excess peak above 1 GeV is about 12 mb. The neutron-excess peak corresponds in width and position to that obtained in fission by ~50-MeV protons. The recoil behavior of Ba^{140} leands support to the idea that the neutron-excess products are formed in a low-deposition-energy process. The recoil behavior of Ba^{131} indicates that it is formed in a high-deposition-energy process. Post-fission neutron evaporation is required to account for the observed characteristics of the excitation functions of the rubidium isotopes and the neutron-deficient species in the Cs region. The correlation between neutron-proton ratios and positions of excitation function maxima is semiquantitatively accounted for if fission with unchanged charge distribution, followed by nucleon evaporation, is assumed.

I. INTRODUCTION

PRESENT knowledge regarding the distribution of nuclear charge and mass in the high-energy fission of uranium is very sparse.[1] The aim of the present study was to obtain information on the dispersion of nuclear charge (i.e., the distribution of fission yields along isobaric chains) which results when uranium fission is induced by protons of various energies.

At low energies, where an abundance of information exists, the most probable product at each mass is neutron rich and is about 3 charge units removed from the line of β stability. The distribution of primary yields about this most probable charge is quite narrow.[2] The total fission yield for each mass can then be obtained by measurement of either the stable or long-lived end products of the β^--decay chains. With increasing bombarding energy, the charge dispersion at a given mass evidently broadens as indicated by the appearance of neutron-deficient nuclides among the fission products.[3] To construct a mass-yield curve it is then necessary to measure chain yields which include contributions from both sides of β stability, and this generally requires detailed knowledge of the isobaric yield distributions in the various mass regions. Furthermore, data on the effect of bombarding energy on isobaric yield patterns can, in themselves, contribute to the elucidation of the fission process.

In this paper, we report a detailed study of cross sections for the independent and cumulative formation of nuclides in the mass range $125<A<140$ in the interaction of uranium with protons of kinetic energies between 0.1 and 6.2 GeV. The results were obtained by a combination of radiochemical and mass-spectrometric techniques. The mass range chosen includes the isotopes of cesium, an element particularly suitable for such a study since there are a relatively large number

* Research performed under the auspices of the U. S. Atomic Energy Commission.
† Present address: State University of New York, Long Island Center, Oyster Bay, New York.
‡ Permanent address: Department of Chemistry, McGill University, Montreal, Canada.
[1] See, for example, the review articles by J. M. Miller and J. Hudis, Ann. Rev. Nucl. Sci. **9**, 159 (1959); and N. A. Perfilov, O. V. Lozhkin, and J. P. Shamov, Uspekhi Fiz. Nauk **60**, 3 (1960) [translation: Soviet Phys.—Uspekhi **3**, 1 (1960)].
[2] A. C. Wahl, R. L. Ferguson, D. R. Nethaway, D. E. Trautner, and K. Wolfsberg, Phys. Rev. **126**, 1112 (1962).
[3] See, for example, A. P. Vinogradov, I. P. Alimarin, V. I. Baranov, A. K. Lavrukhina, T. V. Baranova, F. I. Pavlotskaya, A. A. Bragina, and Yu. V. Yakovlev, *Proceedings of the Conference of the Academy of Sciences of the U.S.S.R. on the Peaceful Uses of Atomic Energy, July 1–5, 1955* (Akad. Nauk, S.S.S.R., Moscow, 1955). U. S. Atomic Energy Commission Report TR-2435, 1956, Part 2, p. 65 (unpublished); and reference 21.

of well-characterized isotopes on both sides of β-stable Cs^{133}. Some of these are so long lived, for example, Cs^{137}, Cs^{135}, and Cs^{134}, that their yields are best determined mass spectrometrically. The yields of short-lived species such as Cs^{125} and Cs^{130} were measured radiochemically. For some isotopes of intermediate half-life (Cs^{127}, Cs^{129}, Cs^{131}, Cs^{132}, and Cs^{136}) both techniques were employed. The mass-spectrometric techniques for the measurement of cesium isotopes at low levels (10^7–10^9 atoms) have previously been described by Gordon and Friedman.[4]

In addition to the direct determination of yields of cesium isotopes, it was possible to obtain data on the formation cross sections of some of the barium, lanthanum, and xenon precursors by separation of cesium at appropriate times.

The mass-spectrometer measurements also yielded relative formation cross sections of some rubidium isotopes, and therefore radiochemical determinations of Rb^{84} and Rb^{86} yields were made.

II. EXPERIMENTAL

1. Irradiations

Irradiations were performed with the circulating proton beams of the Nevis Cyclotron of Columbia University (0.1, 0.2, and 0.38 GeV), the University of Chicago Synchrocyclotron (0.2, 0.3, and 0.45 GeV), the Berkeley 184-in. Cyclotron (0.68 GeV), the Brookhaven Cosmotron (1.0, 2.0, and 2.9 GeV), and the Berkeley Bevatron (6.2 GeV). The targets consisted of natural uranium foils, cleaned with nitric acid prior to irradiation. At the lower bombarding energies ($\leqslant$0.68 GeV) the thickness varied between 0.0005 and 0.001 in., while only 0.001-in. foil was used at the higher energies. In a few early mass-spectrometer measurements 0.0025-in. targets were employed. Irradiation times varied from 5 min to several hours, depending on beam intensities and on particular products investigated. Some of the targets irradiated at Nevis and those irradiated at Berkeley were processed at Brookhaven, and therefore no data on the shorter lived products were obtained from these experiments.

For those irradiations designated for the preparation of mass-spectrometry sources, the proton beam was not monitored, and only relative isotopic yields were determined in these experiments. The target foils in these experiments were always less than 3 mm high. It was found experimentally that the beam is intercepted efficiently by such a target both in the Nevis Cyclotron and in the Cosmotron and that 90% of the interactions take place in an area of about 0.2 cm^2. Thus, no more than 10 mg of uranium had to be dissolved. This was an important factor in keeping the natural cesium contamination to a minimum.

In the radiochemistry experiments, the reaction $Al^{27}(p,3pn)Na^{24}$ was used to monitor the proton beam. A 0.003-in. aluminum monitor foil was placed upstream from the target foil, separated from it by a 0.001-in. aluminum guard foil. In some experiments a similar monitor foil was also placed downstream from the target, again separated from the uranium by a guard foil to check target alignment and possible secondary contributions to the Na^{24} production. Usually these two monitor activities agreed to within 1%, although in one case the disagreement amounted to 5%.

2. Chemical Separations

For the mass-spectrometer measurements it was necessary to remove the uranium efficiently, but not necessary to isolate cesium chemically from the other fission products, since the surface ionization in the spectrometer served as a selective separation process.[4] It was, however, found to be important to keep natural cesium contamination to a minimum to avoid obscuring the neighboring peaks by the tails of a large Cs^{133} peak. Therefore, the chemical procedure was kept as simple as possible, quartz micro-equipment was used throughout, and all reagents were purified by distillation in an all-quartz apparatus. The quartzware was washed with triply distilled water and flamed immediately before use.

The uranium foil was washed rapidly with three separate portions of cold concentrated HNO_3 to remove the oxide layer and any natural cesium contamination on the surface. The foil was then dissolved in 1 ml hot concentrated HNO_3 and the uranium removed by repeated extractions of uranyl nitrate into diethyl ether at 0°C. Nine successive extractions were made, the first with 1 ml of ether, the remainder with 0.5-ml portions, and the phases were separated after centrifugation. After the third, fifth, and seventh extractions, the HNO_3 concentration was replenished by addition of 0.5 ml concentrated HNO_3. After each introduction of fresh HNO_3 the solution was carefully warmed, and air was bubbled through the solution to remove NO_2. This was a necessary precaution to avoid a violent reaction on the subsequent addition of ether. The procedure described reduced the amount of uranium to less than 10^{-4} mg. Tracer experiments with carrier-free Cs^{131} showed that, with care, it was possible to retain more than 60% of the cesium in the final aqueous extract. The final aqueous residue was treated with 1 ml aqua regia in order to remove possible organic impurities which could be troublesome in the mass-spectrometer measurements, if present in amounts very large compared with the amount of cesium. The aqua regia solution was evaporated to dryness in an oven, the residue taken up in about 0.02 ml triply distilled H_2O, transferred to the mass-spectrometer filament, and evaporated under an infrared lamp. Prior to this, the filament had been heated to incandescence and pretreated by the evaporation of a drop of solution containing approximately 0.05 mg $(NH_4)_2SO_4$ which served as a flux to give optimum sensitivity.[4]

[4] B. Gordon and L. Friedman, Phys. Rev. **108**, 1053 (1957).

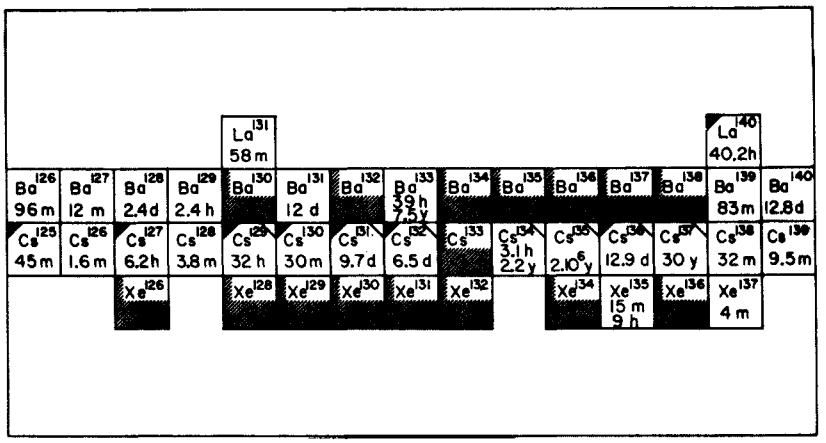

FIG. 1. Nuclides in the cesium region. The nuclides determined mass spectrometrically are indicated by an open triangle in the upper right-hand corner, those measured radiochemically by a filled triangle in the upper left-hand corner. Shaded squares indicate stable nuclides.

The radiochemistry experiments were designed (1) to achieve a quick Ba-Cs separation for separate determinations of independent Cs yields and cumulative yields in the mass 127, 129, and 131 chains; (2) to isolate cesium sufficiently rapidly for the study of short-lived cesium isotopes, and in sufficient radiochemical purity so that the Cs^{136} β^- activity could be measured.

The general procedure used for cesium purification was as follows: The uranium target was dissolved in 12*N* HCl plus a drop of concentrated HNO_3. Carriers for Cs (5 mg), Ba (50 mg), Rb (1 mg), La (1 mg) were added, the solution was made to 3 ml with 12*N* HCl, cooled in ice, and $BaCl_2$ was precipitated by the use of gaseous HCl. The supernate containing the cesium was purified by the following sequence of steps: dilution to 6*N* HCl, precipitation of cesium silicotungstate, washing with 6*N* HCl, dissolution in a minimal volume of 6*N* NaOH, addition of excess acetic acid and rubidium hold-back carrier, and precipitation of $Cs_3Bi_2I_9$ by BiI_3-HI reagent. The final precipitate was washed with 0.1*N* HCl and filtered.

The $BaCl_2$ precipitate was purified by dissolution in H_2O, addition of 1 mg Cs carrier, and reprecipitation of $BaCl_2$ with gaseous HCl. This precipitate was dissolved in H_2O and, after addition of 5 mg cesium and 1 mg rubidium carriers, was set aside for future cesium separations. At appropriate times cesium could be separated from the solution by the above procedure.

In those instances where rubidium was also isolated, 5 mg rubidium carrier was added to the original uranium solution, and rubidium and cesium were precipitated as the perchlorates. The precipitate was dissolved in dilute acetic acid and $Cs_3Bi_2I_9$ was precipitated. This precipitate was treated by dissolution in 12*N* HCl, precipitation of cesium silicotungstate, dissolution in NaOH, purification by a cation-exchange column, and final precipitation as $CsClO_4$. The BiI_3-HI reagent in the supernate from the $Cs_3Bi_2I_9$ precipitation was destroyed by boiling with HNO_3 to drive off iodine and by precipitation of bismuth as oxynitrate. The rubidium was purified by lanthanum hydroxide and barium carbonate scavengings, precipitation of added sodium ion as NaCl, precipitation of $RbClO_4$, conversion to Rb_2SnCl_6 by $SnCl_4$ solution in HCl-C_2H_5OH (this separates rubidium from potassium), dissolution in hot H_2O, removal of tin as SnS_2, and final precipitation of $RbClO_4$.

In some instances La^{140} was extracted from separated barium samples, to which lanthanum carrier had been added, in order to determine chain yields of Ba^{140}. Barium was removed as $BaCl_2$, $La(OH)_3$ precipitated, the precipitate dissolved, and $La_2(C_2O_4)_3$ brought down.

All final precipitates were mounted on filter paper circles by filtration, placed on aluminum or copper cards, and covered with 1 mg/cm^2 Mylar film. After the radioactivity measurements were completed, chemical yields were determined by standard analytical methods. When successive milkings of cesium from barium were made, the chemical yields of barium at each stage had to be determined also.

3. Measurements

A. General

Figures 1 and 2 show the regions of the nuclide chart of interest in this investigation. Measurements were performed on cesium and rubidium isotopes and on La^{140}. In the figures, those nuclides determined mass spectrometrically are indicated by an open triangle in the upper right-hand corner, those measured radiochemically are indicated by a filled triangle in the upper left-hand corner.

Cesium was separated from xenon at the time of target dissolution and from barium at the time of the first $BaCl_2$ precipitation (or at the evaporation from the mass spectrometer filament); these separation times could be appropriately chosen so that either chain or independent yields of various cesium isotopes were obtained. The isotopes Cs^{130}, Cs^{132}, Cs^{134}, and Cs^{136} are shielded by stable Xe and Ba isobars and their yields are, therefore, always independent, except for the

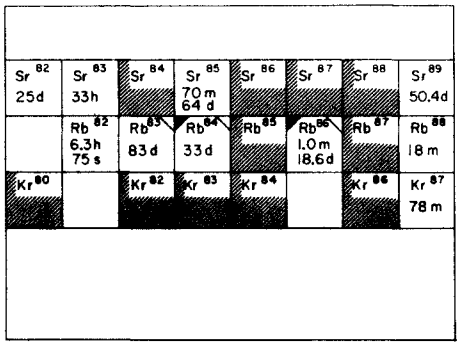

FIG. 2. Nuclides in the rubidium region. The nuclides determined mass spectrometrically are indicated by an open triangle in the upper right-hand corner, those measured radiochemically by a filled triangle in the upper left-hand corner. Shaded squares indicate naturally occurring nuclides.

unlikely possibility that there exist unknown β-emitting isomeric states of these even-even Xe and Ba isotopes. The analogous situation obtains for Rb^{84} and Rb^{86}. The measured yields of 18.6-day Rb^{86} include formation via the 1-min isomer which decays entirely by isomeric transition.[5]

The precursors of Cs^{125}, Cs^{137}, and Ba^{140} are so short lived that only chain yields of these nuclides were determined. Rapid barium-cesium separations allowed the determination of the Cs^{127}, Cs^{129}, and Cs^{131} yields, although corrections for growth from the barium parents during irradiation and prior to separation had to be made. In the radiochemical experiments, cesium milkings from the barium fractions at appropriate later times enabled the Ba^{127}, Ba^{129}, and Ba^{131} chain yields to be determined and these corrections to be made. The irradiation times used in the present work were long enough to make the growth of Cs^{127} from Ba^{127} very substantial, so that independent Cs^{127} formation was not accurately measurable. Variation in the time allowed for Sr^{83}, Ba^{129}, and Ba^{131} decay between irradiation and mass spectrometer measurements provided the information necessary to determine chain and independent yields of Rb^{83}, Cs^{129}, and Cs^{131}. Independent and chain yields of Ba^{131} were obtained radiochemically by extraction of cesium from barium fractions separated immediately after irradiation and after sufficient time for La^{131} decay. The time of dissolution of the uranium targets determined the relative contribution of chain growth and independent formation to the measured Cs^{135} yields. (The 15-min Xe^{135} isomer decays to Cs^{135} entirely[5] via the 9-h ground state of Xe^{135}.)

B. Mass Spectrometry

Mass-spectrometer techniques for isotopic analysis of alkali metals in concentrations of 10^{-10}–10^{-14} g per gram of target material have been briefly described,[4] and these were essentially the techniques finally used in the present work. Various modifications were investigated in an attempt to improve the method. It was initially felt that a major weakness in the procedure is the danger of contamination in handling the samples, loading the filaments, etc. The failures experienced were frequently caused by either excessive natural cesium or barium in the sample or by the presence of unidentified organic compounds. One might expect that interference by the latter could be suppressed by substitution of a filament material of lower work function that would still be adequate for ionization of alkali metals but would reduce the efficiency of ionization of organic or inorganic species of considerably higher ionization potential. The use of rhenium ionization filaments was, therefore, extensively explored. Rhenium was found to be unsuitable for rubidium analyses at low levels because of unidentified ions produced from the ionizing filament in the mass region 80–90. In addition, high yields of ions in the 120–140 mass region were observed when rhenium filaments loaded with pure ammonium sulfate were heated to temperatures very close to those required for the evaporation of cesium. For these reasons, the use of rhenium was abandoned and platinum ionizing filaments were used. Some consideration was given to the possibility that atmospheric dust was in part responsible for the observed sample contaminations. The loading and evaporation of samples on the filaments were normally carried out in the open room. Tests were made on samples loaded directly in the mass-spectrometer tube in an atmosphere of helium. No improvement was noticed and it was concluded that other sources of contamination were at least as important as the exposure to atmospheric dust at this step.

The quantities of Cs^{132} and Cs^{134} produced in the proton irradiations set a limit to the amount of Cs^{133} contamination that could be tolerated. In typical Cosmotron and Bevatron irradiations, of the order of 10^8 atoms of Cs^{132} and Cs^{134} were produced, and the Cs^{133} contamination had to be held below $\sim 10^3$ times this amount. In the synchrocyclotron experiments the number of Cs atoms produced was of the order of 10^{10}–10^{11} atoms; thus one could reduce the collector slit width and, with correspondingly reduced sensitivity, tolerate a ratio of Cs^{133}/Cs^{132} or Cs^{133}/Cs^{134} of 10^4. Slightly larger amounts of natural barium were acceptable as contaminants. When the need for rapid determinations dictated short pumpdown and filament outgassing times, the resulting higher pressures in the mass spectrometer tube set much lower limits to the allowable natural Cs and Ba contamination levels.

C. Radioactivity Measurements

The pertinent properties of the radionuclides measured in this work are given in Table I. Three types of

[5] *Nuclear Data Sheets*, compiled by K. Way *et al.* (Printing and Publishing Office, National Academy of Sciences–National Research Council, Washington 25, D. C.).

TABLE I. Relevant properties[a] of radionuclides measured and modes of detection used.

Nuclide	Half-life	Mode of decay	Maximum β energy (MeV)	Branch abundance	Radiation measured	Instrument used
Cs^{125}	45 min	β^+	2.05, 1.93	0.49[b]	β^+	511-511 Coinc.
		EC		0.51[b]		
Cs^{127}	6.2 h	β^+	0.68, 1.06	0.035[b]	β^+	511-511 Coinc.
		EC		0.965[b]	X	NaI spectrometer
Cs^{129}	32.4 $\pm$0.3 h[c]	EC		1.0	X	NaI spectrometer
Cs^{130}	30 min	β^+	1.97	0.46	β^+	511-511 Coinc.
Cs^{131}	9.69$\pm$0.05 day[d]	EC		1.0	X	NaI spectrometer
Cs^{132}	6.48$\pm$0.03 day[e]	EC		1.0	X	NaI spectrometer
Cs^{136}	12.93$\pm$0.03 day[f]	β^- (γ)	0.34, 0.66	1.0	β^-	End window prop.
Rb^{84}	33 day	β^+ and β^-		0.27[g]	β^+ and β^-	End window prop.
Rb^{86}	18.6 day	β^- (γ)	0.23, 0.71, 1.8	1.0	β^-	End window prop.
La^{140}	40.2 h	β^- (γ)	0.42-2.2	1.0	β^-	End window prop.

[a] Unless otherwise noted, the properties were taken from the *Nuclear Data Sheets*. See reference 5.
[b] G. Friedlander and L. Yaffe, Can. J. Phys. 40, 1249 (1962).
[c] This half-life value was determined from measurements of the decay of seven Cs^{129} samples over six or seven half-lives. These samples were obtained by milking from barium fractions about one day old and were, thus, almost free of other cesium activities.
[d] This half-life value is taken from N. L. Lark and M. L. Perlman, Phys. Rev. 120, 536 (1960). It was independently verified in the present work by measurement of many pure Cs^{131} samples separated from Ba^{131}.
[e] G. N. Whyte, B. Sharma, and H. W. Taylor, Can. J. Phys. 38, 877 (1960).
[f] This half-life value was obtained from measurements over 6 to 8 half-lives, on both end window and 4π β counters, of pure Cs^{136} samples prepared by $Ba^{138}(d,\alpha)$ reaction. It is in excellent agreement with the value 12.9 days given by J. L. Olsen and G. D. O'Kelley, Phys. Rev. 95, 1539 (1954).
[g] J. P. Welker and M. L. Perlman, Phys. Rev. 100, 74 (1955) and (private communication) from M. L. Perlman.

instruments were used: end-window β proportional counters, a NaI crystal (2 mm thick) with single-channel analyzer for x-ray measurements, and a coincidence apparatus for measurement of annihilation radiation from β^+ emitters. The decay of each sample was followed for an appropriate length of time (usually until background rates had almost been reached), and the decay data were analyzed by means of a least-squares computer program devised by Cumming.[6] This program, in addition to giving initial counting rates and their standard deviations for up to ten components, can be used to obtain a least-squares fit of half-lives. The latter feature was used in evaluating the half-lives of Cs^{129}, Cs^{131}, and Cs^{136} listed in Table I.

End-window methane-flow proportional counters were used to measure the counting rates of Cs^{136}, La^{140}, Rb^{84}, and Rb^{86}. The intrinsic counting efficiency of these counters for x rays was found to be very small ($<1\%$ for the Xe K x rays emitted in the decay of Cs^{131}). Generally, the cesium samples decayed with an almost pure 12.93-day half-life after short-lived components had been allowed to decay for a few days. Occasionally, a small unidentified component of 50- to 60-day half-life was present. In order to calibrate the counting efficiency for Cs^{136} radiations, a sample of pure carrier-free Cs^{136} was prepared by irradiation, with 20-MeV deuterons, of barium enriched in Ba^{138} ($\sim 98\%$ abundance[7]). The Cs^{136} was isolated by standard chemical procedures,[8] and the absolute disintegration rate of a measured aliquot was determined in a 4π-β-proportional counter.[9] Other aliquots, mixed with various amounts of cesium carrier, were used to determine the counting efficiencies of the end-window β counters for Cs^{136} in $CsClO_4$ and $Cs_3Bi_2I_9$ samples.

The decay curves of the lanthanum samples separated from barium fractions showed predominantly the 40.2-h half-life of La^{140}. The counting efficiency for La^{140} in $La_2(C_2O_4)_3$ precipitates was determined in a manner analogous to that described for Cs^{136}, with carrier-free La^{140} prepared by thermal-neutron fission of uranium.

The rubidium decay curves could always be cleanly resolved into a dominant 18.6-day component (Rb^{86}), a smaller 33-day component (Rb^{84}), and a very small long-lived tail consistent with the contribution of natural Rb^{87} introduced with the carrier. A high-specific-activity Rb^{86} sample prepared by $Rb^{85}(n,\gamma)$ reaction was used to determine the end-window counter efficiency for Rb^{86} in $RbClO_4$ samples. The counting efficiency for Rb^{84} was estimated on the basis of the known abundances and energies of the β radiations (see Table I). Because of the uncertainty in this estimate, greater reliance was placed on the mass-spectrometric than on the radiochemical determinations in the evaluation of Rb^{84} cross sections.

The K x rays emitted by the cesium isotopes which decay by electron capture were measured with a NaI crystal 2 mm thick and 45 mm in diameter, used in conjunction with a single-channel analyzer set to include the entire x-ray photopeak. The channel settings were frequently checked with pure Cs^{131} sources, and a Cs^{137} standard was used to insure day-to-day constancy of response. (With the channel set for Xe x rays, the Ba x rays emitted by Cs^{137} provided a sensitive indication of channel drifts.) The background rate was approximately 2 counts per minute. Decay curves of cesium samples isolated directly from the target solutions were

[6] J. B. Cumming, Brookhaven National Laboratory Report BNL 6470, 1962 (unpublished).
[7] Obtained from Union Carbide Nuclear Company, Oak Ridge National Laboratory.
[8] E. K. Hyde, J. Am. Chem. Soc. 74, 4181 (1952).
[9] R. Withnell, Nucl. Instr. Methods 14, 279 (1961).

so complex that analysis of components with short half-lives (<6 h) was not attempted. The computer program was used to analyze the curves into half-life components of 6.2 h (Cs^{127}), 32.4 h (Cs^{129}), 6.48 day (Cs^{132}), 9.69 day (Cs^{131}), 12.93 day (Cs^{136}), and a longer lived tail. The contributions of 18-h Xe^{125} and 36.4-day Xe^{127} to the x-ray activity as a function of time were calculated from the β^+ activity of Cs^{125} and the x-ray activity of Cs^{127} at the time of the last Cs-Xe separation. These contributions were subtracted from the gross x-ray activity and the resultant data were again subjected to decay curve analysis, this entire procedure being performed by the computer program. Resolution of Cs^{132} and Cs^{131} was further aided by subtraction of the Cs^{136} contribution determined from the β^- measurement and the measured efficiency of the x-ray counter for Cs^{136}. Decay curves of cesium samples separated from barium fractions were much less complex, containing only Cs^{127}, Xe^{127}, Cs^{129}, and Cs^{131} components, in proportions depending on the timing of the separation and on the previous history of the barium fraction.

The over-all efficiency of the x-ray detection equipment for Xe K x rays was measured with a Cs^{131} sample whose K x-ray emission rate had been kindly determined by B. D. Pate with a NaI detector which subtended a well-defined small solid angle. For the conversion of the measured K x-ray emission rates to K-electron capture decay rates, a fluorescence yield of 0.87 [10] was used. The L/K capture ratio was taken as 0.12 [11] independent of decay energy (since all decay energies[5] of interest are large compared to the K-binding energy).

The determination of positron disintegration rates was based on a measurement of coincidences between the two annihilation quanta detected in 2-in.×2-in. NaI crystals. Pulse-height selection was used in conjunction with each detector, with the channel set to accept the 511-keV photopeak. Samples were mounted between copper absorbers of sufficient thickness to ensure annihilation of all positrons in a small volume. The contributions to the coincidence rate by nuclear gamma rays was monitored by measurement with the detectors placed at 90° to each other. This was done either by moving one of the detectors or by simultaneous measurement of 90° and 180° coincidences with three detectors. The 90° coincidence rate was usually less than 10% of the 180° rate and was subtracted from it to obtain the true annihilation coincidence rate. To minimize pulse addition in the crystals which could add to or subtract from the channel rates, the solid angles subtended by the crystals at the source were as small as possible, consistent with source strength (never more than 5% of 4π steradians); for the β^+ emitters studied, the errors due to this effect were usually negligible and never exceeded a few percent.

TABLE II. Cross sections of the monitor reaction $Al^{27}(p,3pn)Na^{24}$.

Proton energy (GeV)	Cross section (mb)
0.10–0.68	10.8
1.0	10.4
2.0	9.5
2.9	9.1
6.2	8.7

With Cs samples produced in the synchrocyclotron irradiations, the coincidence rate decayed with a 30-min half-life (Cs^{130}) into a small tail with a 6.2-h half-life (Cs^{127}). At higher proton energies, the 45-min Cs^{125} component appeared. The efficiency of the coincidence detection system was calibrated with a Na^{22} standard whose disintegration rate had been determined[12] by triple coincidences, β-γ coincidences, and by comparison with a calibrated NBS standard. The fraction of Na^{22} decaying by positron emission was taken to be 0.898.[5]

The Na^{24} monitor activity was measured by end-window proportional counters previously calibrated by β-γ coincidence measurements.

III. RESULTS

1. Treatment of Data

In the radiochemical experiments, the counting rates, either at the end of irradiation, or at time of chemical isolation from the parent, were converted to disintegration rates D^0 by the use of the counter efficiencies, branching ratios, and chemical yields. In those experiments which did not require considerations of parent-daughter relationships (e.g., shielded or effectively shielded nuclides or cumulative yields of long-lived daughters with short-lived parents) the cross section σ was obtained from D^0 at the end of irradiation by means of the equation

$$\sigma = D^\infty F, \tag{1}$$

where

$$F = \frac{W_{Al}}{W_U}\frac{A_U}{A_{Al}}\frac{\sigma_{Al}(Na^{24})}{D^\infty{}_{Na^{24}}},$$

and

$$D^\infty = D^0/(1-e^{-\lambda t_0});$$

λ=decay constant of the nuclide in question, t_0=length of irradiation,[13] $D^\infty{}_{Na^{24}} = D^0{}_{Na^{24}}/[1-\exp(-\lambda_{Na^{24}} t_0)]$, W_{Al} and W_U are the superficial densities of the alumi-

[10] A. H. Wapstra, G. J. Nijgh, and R. Van Lieshout, *Nuclear Spectroscopy Tables* (Interscience Publishers, Inc., New York, 1959).

[11] H. Brysk and M. E. Rose, Rev. Mod. Phys. **30**, 1169 (1958).

[12] We are grateful to Dr. J. B. Cumming, Dr. N. T. Porile, Dr. A. M. Poskanzer, and Dr. L. Remsberg for supplying their data on these calibrations.

[13] In a few instances, where t_0 was not short compared to the half-life, the saturation factor $(1-e^{-\lambda t_0})$ was appropriately corrected for variations in beam intensity during irradiations.

num and uranium foils, A_{Al} and A_U are the atomic weights of aluminum and uranium, $\sigma_{Al}(Na^{24})$ is the cross section for production of Na^{24} in aluminum, and $D^0_{Na^{24}}$ is the disintegration rate of Na^{24} in the aluminum foil at end of irradiation.

The values of the monitor cross section, $\sigma_{Al}(Na^{24})$ used in this work, are given in Table II. For energies above 0.3 GeV, they are based on the analysis of Cumming *et al.*[14] From 0.1 to 0.3 GeV, $\sigma_{Al}(Na^{24})$ was for simplicity assumed to be constant at 10.8 mb, although there is evidence[15] for a shallow ($\sim 10\%$) dip in the excitation function in the region of 0.2 GeV.

When both members of a parent-daughter pair are produced independently with cross section σ_p and σ_d, respectively, in an irradiation of duration t_0, the disintegration rate $D_d{}^1$ of the daughter at time t_1 after the end of irradiation is given by

$$D_d{}^1=(\lambda_d/F)(K_1\sigma_p+K_2\sigma_d), \tag{2}$$

where F is, as defined in Eq. (1),

$$K_1=\frac{e^{-\lambda_p t_1}(1-e^{-\lambda_p t_0})-(\lambda_p/\lambda_d)e^{-\lambda_d t_1}(1-e^{-\lambda_d t_0})}{\lambda_d-\lambda_p},$$

$$K_2=\frac{e^{-\lambda_d t_1}(1-e^{-\lambda_d t_0})}{\lambda_d},$$

and λ_d and λ_p are the decay constants of the daughter and parent, respectively.

For most of the parent-daughter pairs investigated here, it was possible to determine σ_p and σ_d either from two separate irradiations with appropriately chosen times t_0 and t_1, each leading to an equation of the form of Eq. (2), or from a single irradiation followed by two successive separations of the daughter product. In the latter case, the daughter activity obtained in the second extraction was used to find σ_p in standard fashion, and σ_d could then be determined by means of Eq. (2) from the daughter activity obtained in the first extraction.

In the mass-spectrometric measurements, the Cs isotopic abundances were determined relative to Cs^{136}, the Rb abundances relative to Rb^{86}. Where parent-daughter relationships are not relevant, the atom ratios, corrected for decay during and after irradiation, directly give the cross-section ratios. The average values of the Cs^{136} and Rb^{86} cross sections determined radiochemically were used to normalize the mass-spectrometer data at each bombarding energy.

Where parent-daughter relationships had to be taken into account (Cs^{129}, Cs^{131}, Cs^{135}, and Rb^{83}), the following modified form of Eq. (2) was applied:

$$N_d{}^1/N_s{}^1=[\lambda_d/(1-e^{-\lambda_d t_0})][K_1(\sigma_p/\sigma_s)+K_2(\sigma_d/\sigma_s)],$$

where $N_d{}^1$ and $N_s{}^1$ are the numbers of atoms of daughter substance and standard (Cs^{136} or Rb^{86}), respectively, at t_1, and σ_s is the cross section for formation of the standard substance. The time t_1 corresponds to the time of target dissolution for the Xe^{135}-Cs^{135} pair, and to the time of measurement for the Ba-Cs and Sr-Rb pairs (because the surface ionization process served to separate these pairs).

[14] J. B. Cumming, J. Hudis, A. M. Poskanzer, and S. Kaufman, Phys. Rev. **128**, 2392 (1962).
[15] H. P. Yule and A. Turkevich, Phys. Rev. **118**, 1591 (1960).

TABLE III. Recoil behavior of Ba^{131} and Ba^{140}.

Proton energy (GeV)	Nuclide	F_FW (mg/cm²)	F_BW (mg/cm²)	$(F_F+F_B)W$ (mg/cm²)	F_F/F_B
0.38	Ba^{131}	2.00	1.55	3.55	1.30
	Ba^{140}	2.12	2.15	4.27	0.99
2.9	Ba^{131}	1.93	1.02	2.95	1.89
	Ba^{140}	2.21	2.01	4.22	1.09

2. Recoil Losses and Secondary Effects

Since rather thin uranium foils were used throughout this work (20 to 50 mg/cm²), it was necessary to correct all measured cross sections for recoil losses. Over a small range of product masses the recoil losses were found not to vary greatly (see below). Therefore, the relative cross sections determined mass spectrometrically were subject to much smaller recoil-loss corrections than the absolute radiochemical results.

To determine the magnitude of the recoil-loss corrections for both neutron-excess and neutron-deficient species, irradiations of a 25 mg/cm² and a 41 mg/cm² uranium foil were carried out at 0.38 and 2.9 GeV, respectively, with aluminum catcher foils both upstream and downstream of the uranium foils. Barium fractions were isolated from each of the catcher and uranium foils, and Ba^{131} and Ba^{140} were determined via the Cs^{131} and La^{140} daughters. The results of these experiments are given in Table III, expressed in terms of the product of the target thickness W (in mg/cm²) and the fractions F_F and F_B recoiling out of the target in the forward and backward directions. These data are thought to be reliable to $\pm 5\%$.

It is seen from column 5 of Table III that the recoil loss of Ba^{140} is essentially energy independent over this range and that the recoil loss of Ba^{131} decreases only about 15% from 0.38 to 2.9 GeV. For purposes of correction, the 2.9-GeV recoil-loss data were used at proton energies of 1.0 to 6.2 GeV, the 0.38-GeV recoil-loss data at all energies from 0.1 to 0.45 GeV; interpolated values were employed to correct the 0.68-GeV cross sections. To obtain recoil-loss corrections for other mass numbers in the range $125 \leqslant A \leqslant 140$, linear dependence of $(F_F+F_B)W$ on A was assumed; any Z dependence was ignored.

No experimental determination of recoil losses in the rubidium region was carried out. For all rubidium isotopes, values of $(F_F+F_B)W$ ranging from 5.2 mg/cm² at 6.2 GeV to 5.7 mg/cm² at 0.68 GeV were used, based

TABLE IV. Formation cross sections at proton energies from 0.10 to 0.45 GeV.

		E_p =0.10 GeV		E_p =0.20 GeV		E_p =0.30 GeV		E_p =0.38 GeV		E_p =0.45 GeV	
Product	Type of yield[a]	Determinations[b]	Cross section (mb)	Determinations[b]	Cross section (mb)	Determinations[b]	Cross section (mb)	Determinations[b]	Cross section (mb)	Determinations[b]	Cross section (mb)
Ba^{140}	C	$R2$	25.4 ±0.4	$R2$	19.1 ±0.1			$R3$	14.6 ±0.4		
Cs^{137}	C	$M1$	37 ±1	$M3$	23.0 ±0.5	$M3$	16.8±0.6	$M2$	16.7 ±0.2	$M3$	14.1±0.7
Cs^{136}	I	$R3$	14.7 ±1.3	$R3$	9.9 ±0.6			$R3$	7.2 ±0.1		
Cs^{135}	C	$M1$	52 ±2	$M2$	33.8 ±1.5	$M3$	24.7±0.8	$M2$	25.4 ±0.1	$M3$	20.7±0.9
Cs^{134}	I	$M1$	11.0 ±0.3	$M3$	8.6 ±0.4	$M3$	7.4±0.3	$M2$	6.9 ±0.1	$M3$	6.7±0.1
Cs^{132}	I	$R2$	3.7 ±0.3	$R3$	5.0 ±0.5	$M3$	6.5±0.1	$R2$	6.2 ±0.3	$M3$	7.1±0.8
		$M1$	3.8 ±0.2	$M2$	4.8 ±0.2			$M2$	6.2 ±0.1		
		Av	3.7 ±0.2	Av	4.9 ±0.4			Av	6.2 ±0.2		
Cs^{131}	I	$M1$	1.47±0.06	$M3$	3.8 ±0.4	$M1$	5.1±0.5	$M2$	6.5 ±0.6		
		$R2$	1.56±0.13	($R2$	5.2 ±0.9)			$R3$	7.1 ±1.0		
		Av	1.53±0.10	Av	3.8 ±0.4			Av	6.5 ±0.9		
Ba^{131}	I	$R1$	0.03±0.01	$R1$	0.7 ±0.1			$R1$	1.9 ±0.1		
	C					$M1$	2.2±0.7	$R2$	2.69±0.02		
La^{131}	C	$R1$	~0.01	$R1$	<0.09			$R1$	0.8 ±0.1		
Cs^{130}	I	$R1$	0.58±0.05	$R2$	2.2 ±0.4			$R2$	5.1 ±0.9		
Cs^{129}	I			$R1$	1.55±0.04			$R1$	3.9 ±0.2		
	C	$R2$	0.05±0.03	$R1$	1.7 ±0.3			$R1$	4.8 ±0.2		
Ba^{129}	C	$R1$	(1.7±0.2) ×10^{-3}	$R1$	0.12±0.01			$R1$	0.90±0.05		
Cs^{127}	C	$R1$	<0.12	$R1$	0.3 ±0.1			$R3$	1.21±0.05		
Cs^{125}	C							$R1$	<0.06		
Rb^{87}	C	$M1$	10 ±3	$M1$	20 ±2			$M1$	41 ±3		
Rb^{86}	I	$R1$	0.6 ±0.2	$R1$	2.3 ±0.1			$R2$	5.6 ±0.7		
Rb^{84}	I	$M1$	<0.04	$M1$	0.8 ±0.1			$R2$	1.7 ±0.3	$M1$	2.0±0.1
								$M1$	1.7 ±0.2		
								Av	1.7 ±0.2		
Rb^{83}	C							$M1$	<0.6	$M1$	1.4±0.1

[a] C =cumulative yield; I =independent yield.
[b] M =mass-spectrometric method; R =radiochemical method. The number following a symbol indicates the number of independent determinations. When more than one determination was made, the error shown is the mean deviation of the individual results from the weighted average. For single determinations, an estimate of the accuracy is indicated (see text).

on interpolations of the data of Alexander *et al.*[16] For proton energies of 0.38 and 0.45 GeV, a value of 6.0 mg/cm² was deduced from unpublished data of Sugarman,[17] for 0.10 and 0.20 GeV a value of 5.5 mg/cm² from data of Noshkin.[18]

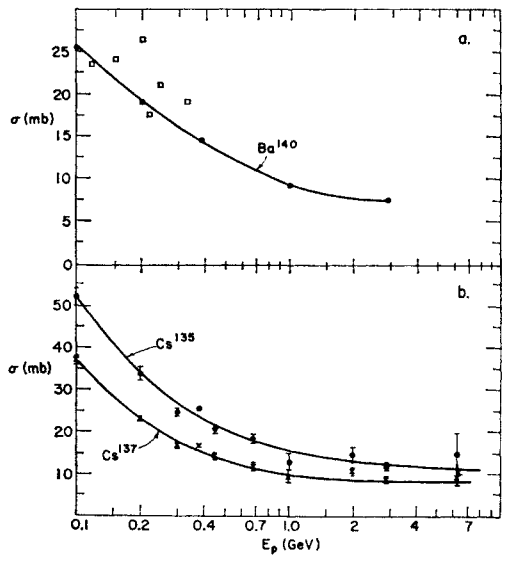

FIG. 3. Excitation functions for cumulative formation of neutron-excess nuclides. (a) Ba^{140}. The open squares are data from reference 22, normalized to the Al(p,3pn) cross sections used in the present paper. (b) Cs^{135} and Cs^{137}.

For the target thicknesses used (W=20 to 50 mg/cm²), the recoil-loss corrections (F_F+F_B) were in the range of 0.06 to 0.20.

Some of the products measured in the present study are formed in high yield in the fission of uranium by low-energy neutrons, which are produced in copious amounts in interactions of high-energy protons with uranium. It was, therefore, necessary to determine the extent to which secondary reactions contribute to the observed cross sections. Several irradiations were made at 3 GeV with uranium foils of various thicknesses ranging from 20 to 325 mg/cm²,[19] and the yields of Ba^{140}, a typical low-energy fission product, were determined. In these experiments, aluminum catcher foils were dissolved together with the target foil, to obviate the need for recoil-loss corrections. The secondary effect observed was small, of the order of 7% per 100 mg/cm² target thickness, and consistent with linear thickness dependence over the range measured. No secondary corrections were applied to most cross-section measurements, since target thicknesses were less than 50 mg/cm². Cross sections of Cs^{135} and Cs^{137}

[16] J. M. Alexander, C. Baltzinger, and M. F. Gazdik, following paper [Phys. Rev. 129, 1826 (1963)].

[17] C. Baltzinger, University of California Radiation Laboratory Report UCRL-8430, 1958 (unpublished).

[18] V. E. Noshkin, Jr., Clark University Annual Report Contract AT(30-1) 1930, 1961 (unpublished).

[19] The results for the 325 mg/cm² foil were kindly made available by Dr. I. Dostrovsky.

TABLE V. Formation cross sections at proton energies from 0.68 to 6.2 GeV.

Product	Type of yield[a]	E_p = 0.68 GeV Determinations[b]	E_p = 0.68 GeV Cross section (mb)	E_p = 1.0 GeV Determinations[b]	E_p = 1.0 GeV Cross section (mb)	E_p = 2.0 GeV Determinations[b]	E_p = 2.0 GeV Cross section (mb)	E_p = 2.9 GeV Determinations[b]	E_p = 2.9 GeV Cross section (mb)	E_p = 6.2 GeV Determinations[b]	E_p = 6.2 GeV Cross section (mb)
Ba^{140}	C			R1	9.3 ±0.6			R3	7.9 ±0.2		
Cs^{137}	C	M1	11.9 ±0.9	M1	9.6 ±1.5	M4	10.8 ±0.6	M3	8.8 ±0.5	M1	9.4 ±1.8
Cs^{136}	I	R1	4.8 ±0.5	R3	4.4 ±0.3	R3	3.6 ±0.4	R2	3.20 ±0.05	R1	2.9 ±0.3
Cs^{135}	I					M1	3.4 ±1.0	M2	2.0 ±0.6		
	C	M1	18.3 ±1.0	M1	13 ±2	M3	14.7 ±1.7	M2	12.0 ±0.2	M1	15 ±5
Cs^{134}	I	M1	5.5 ±0.3	M1	3.0 ±0.5	M3	3.1 ±0.4	M3	2.8 ±0.1		
Cs^{132}	I	R1	5.4 ±1.0	R3	4.2 ±0.3	R3	3.4 ±0.5	R2	3.3 ±0.2		
		M1	6.0 ±0.3	M1	3.5 ±0.5	M3	3.9 ±0.1	M2	3.2 ±0.1		
		Av	5.9 ±0.3	Av	4.1 ±0.4	Av	3.8 ±0.4	Av	3.3 ±0.15		
Cs^{131}	I	RM1	5.8 ±0.3	R3	5.7 ±0.8	R2	3.6 ±0.3	R1	3.2 ±0.4	RM1	2.4 ±1.1
				M1	4.4 ±0.6	RM1	4.1 ±0.2	M1	4.1 ±0.4		
				Av	5.4 ±0.9	Av	3.8 ±0.3	RM2	3.7 ±0.5		
								Av	3.7 ±0.4		
Ba^{131}	I			R2	3.4 ±0.1	R2	2.40 ±0.05	R2	2.55 ±0.05		
	C	RM1	6.2 ±0.3	(M1	4.0 ±1.7)	(RM1	7.9 ±1.8)	R2	8.55 ±0.05	RM1	6.6 ±0.9
				R1	5.8 ±0.2	R1	6.8 ±0.2				
				Av	5.8 ±0.2	Av	6.8 ±0.2				
La^{131}	C			R2	2.4 ±0.1	R2	4.40 ±0.05	R2	6.0 ±0 1		
Cs^{130}	I			R2	5.55 ±0.05	R2	4.3 ±0.2	R2	4.3 ±0.1		
Cs^{129}	I			R2	6.45 ±0.05	R2	4.9 ±0.8	R2	5.0 ±0.5		
	C	M1	6.4 ±0.4	R1	9.4 ±0.3					M1	13 ±3
Ba^{129}	C			R2	3.60 ±0.05	R1	5.5 ±0.2	R1	6.7 ±0.3		
						M1	5.0 ±0.5	(RM2	4.1 ±0.6)		
						Av	5.4 ±0.2	Av	6.7 ±0.3		
Cs^{127}	I			R2	3.0 ±0.2			R1	2.8 ±0.5		
	C			R2	4.4 ±0.4	R2	7.0 ±0.8	R1	6.8 ±0.6		
						M1	7.3 ±0.4	M1	7.1 ±1.0		
						Av	7.2 ±0.6	Av	6.9 ±0.2		
Ba^{127}	C			R2	1.4 ±0.4			R1	4.7 ±0.4		
Cs^{125}	C			R2	1.1 ±0.1	R2	2.7 ±0.5	R2	3.9 ±0.2		
Rb^{86}	I	R1	8.3 ±0.5	R1	10.8 ±0.7	R1	9.5 ±0.6	R1	8.5 ±0.5	R1	6.9 ±0.4
Rb^{84}	I	M1	3.6 ±1.2	R1	6.9 ±0.7	(R1	8.0 ±1.0)	(R1	7.8 ±1.0)	R1	5.2 ±1.1
						M2	6.9 ±0.1	M2	5.4 ±0.3		
						Av	6.9 ±0.1	Av	5.4 ±0.3		
Rb^{83}	I	M1	<2.4			M1	6.2 ±0.7	M1	3.9 ±0.4		
	C	M1	3.6 ±1.2								

[a] C = cumulative yield; I = independent yield.
[b] M = mass-spectrometric experiment; R = radiochemical experiment; RM indicates result obtained by combining data from a radiochemical and a mass-spectrometric experiment. The number following a symbol indicates the number of independent determinations. When more than one determination was made, the error shown is the mean deviation of the individual results from the weighted average. For single determinations, an estimate of the accuracy is indicated (see text).

(cumulative), determined in a few early irradiations of ~100 mg/cm² foils, were decreased by 7% to correct for production by secondaries.

3. Cross Sections and Excitation Functions

The formation cross sections for the various nuclides are given in Tables IV and V. The symbols *M* and *R* denote mass-spectrometric and radiochemical measurements, respectively; the number following each symbol indicates the number of determinations. In general, agreement between the two methods was gratifying whenever a cross section could be determined both ways. The formation cross sections of certain products, although determined in both types of experiments, are more reliably obtained from one or the other. In particular, because of the difficult resolution of x-ray decay curves with 6.48-day, 9.69-day, and 12.93-day components, the cross sections for independent formation of Cs^{131} and Cs^{132} are better determined mass spectrometrically than radiochemically. On the other hand, the radiochemical measurement of cumulative Ba^{129} and Ba^{131} cross sections could be done in very straightforward manner and led to more reliable results than did the corresponding mass spectrometry. In three of the mass spectrometer experiments the small Cs^{136} peak was not sufficiently well resolved from the large neighboring 135 and 137 peaks to serve as the basis of reliable isotope ratios; in these cases, the isotope ratios were determined relative to Cs^{127}, and the cumulative Cs^{127} cross sections, determined radiochemically, were used to convert isotope ratios to cross sections. At proton energies of 0.1, 0.2, and 0.38 GeV, the mass-spectrometrically observed Rb^{87}/Rb^{85} ratio differed sufficiently from the normal abundance ratio to allow an estimation of the Rb^{87} formation cross section (see Table IV).

Errors for individual radiochemical results were estimated from the uncertainties in decay curve analyses, counting efficiencies, and chemical yields. Standard deviations for individual mass-spectrometer experiments were obtained by statistical treatment of the mass ratios in repeated scans, and do not reflect the uncertainties in the radiochemically determined Cs^{136}

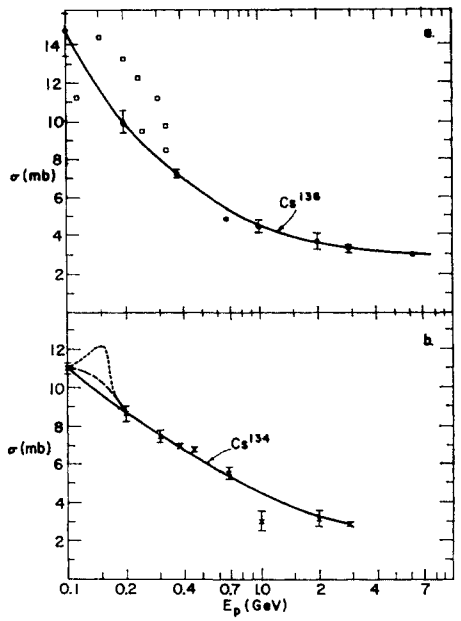

FIG. 4. Excitation functions for independent formation of neutron-excess nuclides. (a) Cs^{136}. The open squares are data from reference 22, normalized to the Al(p,3pn) cross sections used in the present paper. (b) Cs^{134}. The dashed lines indicate other possible interpolations as discussed in the text.

and Rb^{86} cross sections. Where the result of a single determination appears in Tables IV and V, the estimated error is given. Otherwise, average values (obtained by weighting the individual results by the reciprocals of their errors) are shown, along with mean deviations calculated without weighting factors. Some results were considered so distinctly less reliable than others (for reasons given in the preceding paragraph) that they were not included in the averages; such data are given in parentheses. The deviations of individual results from the averages were generally quite comparable to the estimated errors on the individual determinations.

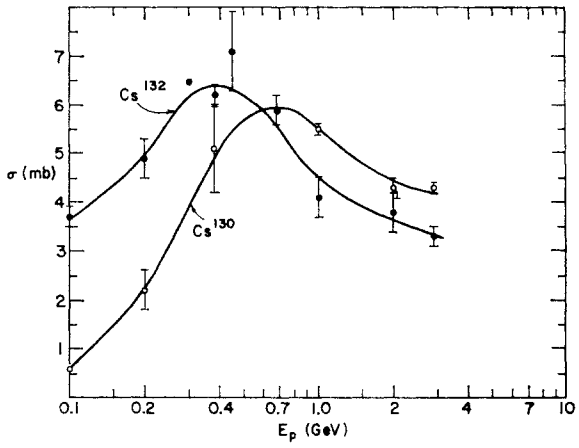

FIG. 5. Excitation functions for independent formation of Cs^{130} (open circles) and Cs^{132} (full circles).

Only mass-spectrometric measurements were obtained at 0.3 and 0.45 GeV bombardment energies. The data, shown in columns 8 and 12 of Table IV, for these irradiations have been normalized to Cs^{136} and Rb^{86} cross sections which were interpolated from the respective excitation functions.

Excitation functions for the various products investigated are shown in Figs. 3 to 8. The errors shown are the average deviations from the mean given in Tables IV and V. The cross sections both for the cumulative (Fig. 3) and independent formation (Fig. 4) of neutron-excess products in the Cs-Ba region are seen to decrease monotonically with increasing energy. The excitation functions for the independent formation

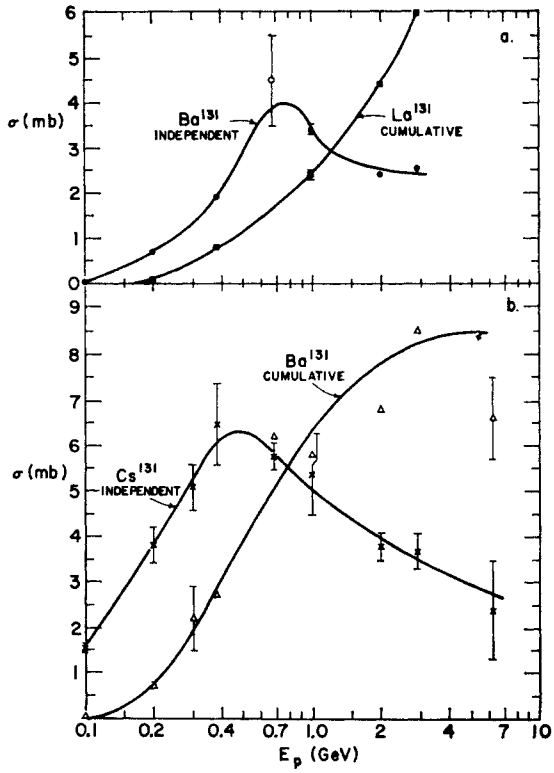

FIG. 6. Excitation functions for isobars in the $A=131$ chain. (a) Independent formation of Ba^{131} (full circles) and cumulative formation of La^{131} (full squares). The point for Ba^{131} at 0.68 GeV was obtained by a subtraction of the cumulative La^{131} cross section (read off the curve) from the measured cumulative Ba^{131} cross section. (b) Independent formation of Cs^{131} (crosses) and cumulative formation of Ba^{131} (open triangles).

of neutron-deficient species in this region and those for the Rb isotopes exhibit maxima as shown in Figs. 5–8. In Figs. 6 and 7, excitation functions for some of the cumulative formation cross sections are also shown; these cross sections generally increase in the energy range investigated. As the bombarding energy is increased, the products with lower neutron-proton ratios become more prominent. Such a trend has been

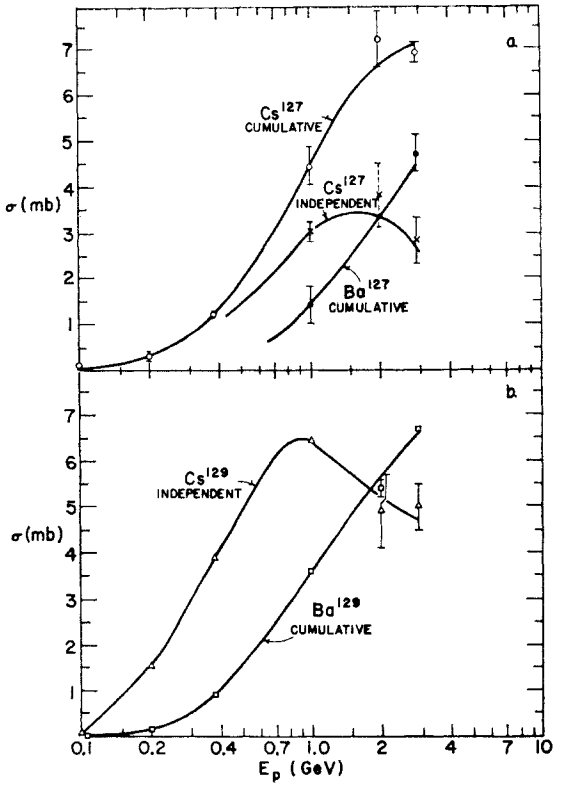

FIG. 7. Excitation functions for isobars in the $A=127$ and $A=129$ chains. (a) Independent formation of Cs^{127} (crosses), cumulative formation of Ba^{127} (full circles), and cumulative formation of Cs^{127} (open circles). The point for the independent formation of Cs^{127} at 2.0 GeV was obtained by subtraction of the cumulative Ba^{127} cross section (read off the curve) from the measured cumulative Cs^{127} cross section. (b) Independent formation of Cs^{129} (triangles) and cumulative formation of Ba^{129} (squares).

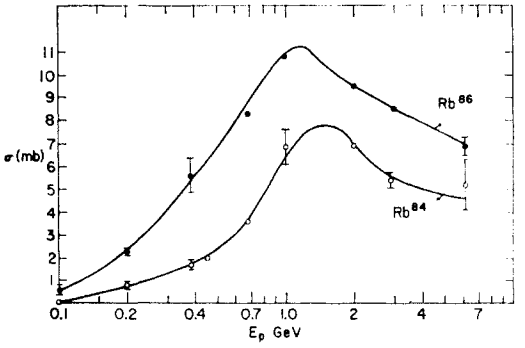

FIG. 8. Excitation functions for the independent formation of Rb^{84} (open circles) and Rb^{86} (full circles).

postulated by Folger *et al.*[20] and Lindner and Osborne[21] and some data to substantiate this point have been given by Hicks and Gilbert.[22] Our results show this effect particularly clearly, as indicated by the fact that the energies at which the excitation functions for the *independent* formation of various products reach their maxima increase with decreasing neutron-proton ratio. In Fig. 9(a), these peak energies are plotted against the N/Z values of the nuclides in question. For comparison, in Fig. 9(b), the same peak energies are plotted against $(Z-Z_A)$, where Z_A is the most stable charge for a given A value, as given by Coryell.[23] The errors shown in the figures indicate the maximum uncertainties in peak position. The cesium data fall on a smooth curve in either representation. It is interesting to note, however, that the rubidium data fit well on the same curve with the cesium points on the N/Z plot, but fall far off on the $(Z-Z_A)$ graph. Thus, the shapes of the excitation functions appear to be correlated with neutron-proton composition rather than with distance from β stability. Extrapolation of Fig. 9(a) to higher N/Z values would indicate that the Cs^{134} excitation function should attain a maximum value between 0.10 and 0.15 GeV. As shown by the dashed curves in Fig. 4(b), this is consistent with our data.

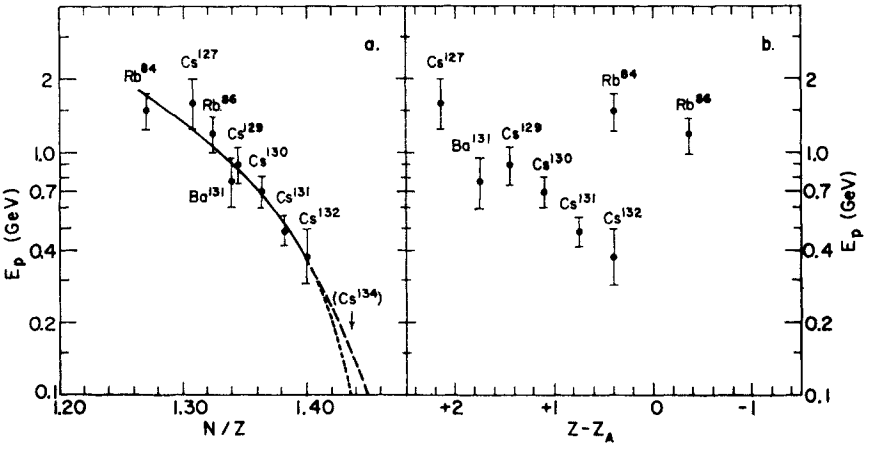

FIG. 9. Energies at which the excitation functions reach maxima (a) as a function of N/Z, (b) as a function of $Z-Z_A$. Z_A values are those of Coryell (reference 23).

[20] R. L. Folger, P. C. Stevenson, and G. T. Seaborg, Phys. Rev. **98**, 107 (1955).
[21] M. Lindner and R. N. Osborne, Phys. Rev. **94**, 1323 (1954).
[22] H. G. Hicks and R. S. Gilbert, Phys. Rev. **100**, 1286 (1955).
[23] C. D. Coryell, Ann. Rev. Nucl. Sci. **2**, 305 (1953).

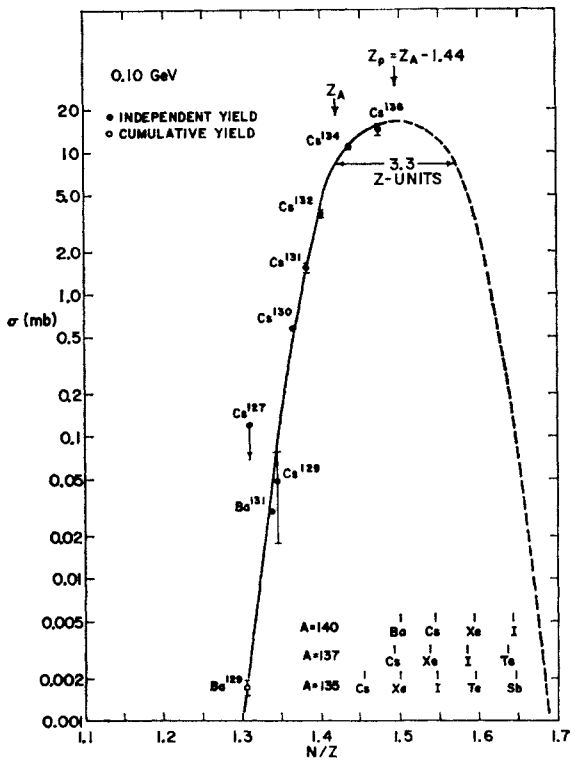

FIG. 10. Charge dispersion at 0.10 GeV. The curve was arbitrarily assumed to be symmetrical. The right-hand (dashed) portion has been drawn so that the sums of the isobaric yields read off the curve approximate the *measured* cumulative yields:

	Experimental σ (mb)	Curve σ (mb)
Cs^{135}	52	47
Cs^{137}	37	37
Ba^{140}	25.4	33

The N/Z values of the isobars contributing to these chain yields are indicated near the bottom.

4. Charge Dispersion

The cross-section data given in Tables IV and V can also be used to obtain information regarding the isobaric yield patterns for the mass range 125–140 at these energies. If one assumes that the mass-yield curve is sensibly flat in this restricted mass range, then the data can be used to construct charge-dispersion curves. Such curves are presented in Figs. 10–17 for the energy range 0.10 to 2.9 GeV. Corroborative evidence for the assumption of "flat" mass-yield curves comes from the fact that the iodine data of Alexander *et al.*[16] for the mass range 121–135 fall smoothly on our curves (see, e.g., Fig. 17), even though the N/Z value of any iodine isotope corresponds to that of a cesium isotope of mass number some five units higher.

The charge dispersion curves are based in the first instance on independent formation cross sections. In those regions where no such data were available (the wings of the curves), the cumulative yields were found extremely useful in defining the shapes of the curves,

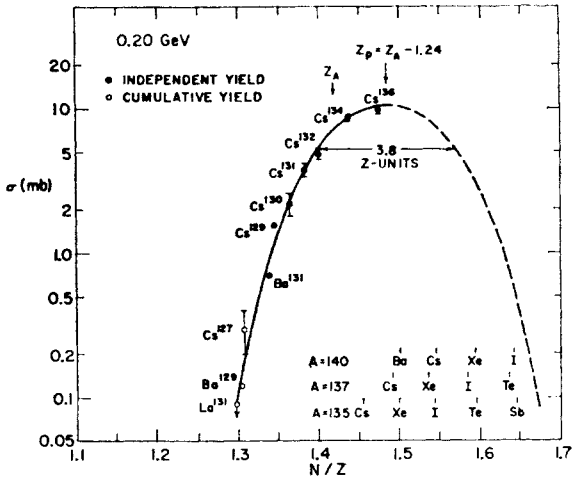

FIG. 11. Charge dispersion at 0.20 GeV. The curve was arbitrarily assumed to be symmetrical. The right-hand (dashed) portion has been drawn so that the sums of the isobaric yields read off the curve approximate the *measured* cumulative yields:

	Experimental σ (mb)	Curve σ (mb)
Cs^{135}	33.8	30.9
Cs^{137}	23.0	23.4
Ba^{140}	19.1	21.8

The N/Z values of the isobars contributing to these chain yields are indicated near the bottom.

since the *interpolated* primary yields for each isobaric chain have to sum to the *measured* cumulative yield for that chain. The relatively poor agreement between measured and interpolated cumulative yields at 0.1 GeV (Fig. 10) may indicate that the assumption of a flat mass-yield curve is not quite justified at this low energy.

In these charge-dispersion curves, the cross sections have been plotted against N/Z, rather than the con-

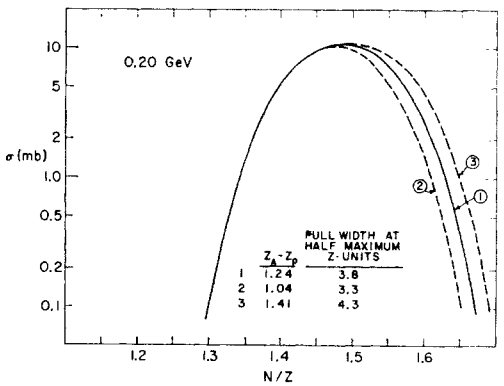

FIG. 12. Charge-dispersion curve at 0.20 GeV, extrapolated in three different ways to show how cumulative yields define the right-hand portion. Curve 1 is identical with that drawn in Fig. 11. The sums of isobaric cross sections (in mb) read off the curves are

	1	2	3	Experimental
Cs^{135}	30.9	26.8	35.7	33.8
Cs^{137}	23.4	19.2	28.2	23.0
Ba^{140}	21.8	17.5	26.5	19.1

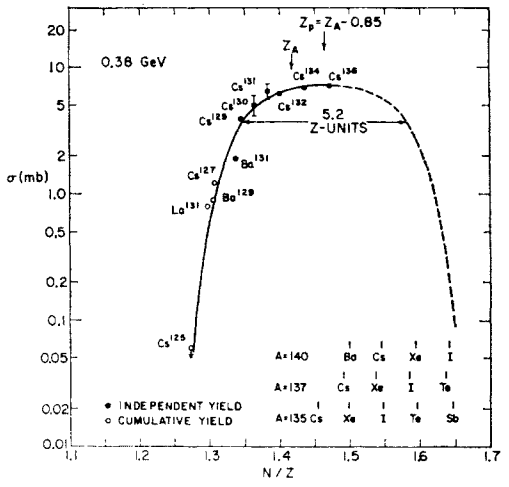

FIG. 13. Charge dispersion at 0.38 GeV. The curve was arbitrarily assumed to be symmetrical. The right-hand (dashed) portion has been drawn so that the sums of the isobaric yields read off the curve approximate the *measured* cumulative yields:

	Experimental σ (mb)	Curve σ (mb)
Cs^{135}	25.4	23.0
Cs^{137}	16.7	17.2
Ba^{140}	14.6	15.8

The N/Z values of the isobars contributing to these chain yields are indicated near the bottom.

ventional $(Z-Z_A)$. That this does not alter the general features of the curves is illustrated in Figs. 17 and 18, where the same data (2.9 GeV) are plotted in both ways. Difficulties were encountered if one invoked the well-known discontinuity[23] at the $N=82$ shell edge. The

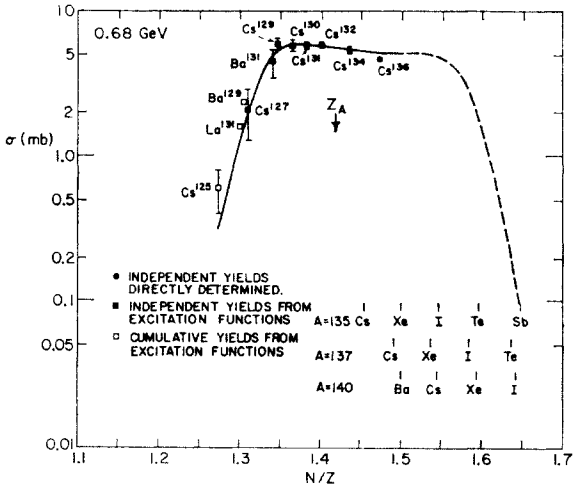

FIG. 14. Charge dispersion at 0.68 GeV. The right-hand (dashed) portion of the curve has been drawn so that the sums of the isobaric yields read off the curve approximate the measured cumulative yields:

	Experimental σ (mb)	Curve σ (mb)
Cs^{135}	18.3	17.4
Cs^{137}	11.9	13.3
Ba^{140}	11.7 (from excitation function)	12.2

TABLE VI. Parameters of charge-dispersion curves observed at the lower bombarding energies.

Proton energy (GeV)	Full width at half-maximum N/Z	Full width at half-maximum Z	Peak position N/Z	Peak position Z_A-Z_P
0.10	0.152	3.3	1.495	1.44
0.20	0.170	3.8	1.485	1.24
0.38	0.234	5.2	1.465	0.85

curve shown in Fig. 18 was drawn in such a way that the cumulative yields for Cs^{135}, Cs^{137}, and Ba^{140} are accounted for if the Z_A values[28] at these mass numbers are those appropriate for $N<82$. A single smooth curve encompassing all the data cannot be drawn if a change of Z_A at the shell edge is assumed. No such difficulties arise if one simply uses the neutron-proton ratio.

In Figs. 10, 11, and 13–18, the independent yields and some upper limits for independent yields are plotted with the errors from Tables IV and V. In some instances, data interpolated from excitation functions were used. In each figure caption are given the experimental cumulative values used in defining the wings of the curve, along with the corresponding sums of independent yields read off the curve. The shape of the curve is defined within narrow limits by these cumulative cross sections. This is illustrated in Fig. 12 which reproduces the 0.2-GeV curve from Fig. 11 along with two other extrapolations which give values for the Cs^{135}, Cs^{137}, and Ba^{140} cumulative cross sections clearly outside the limits of the experimental data.

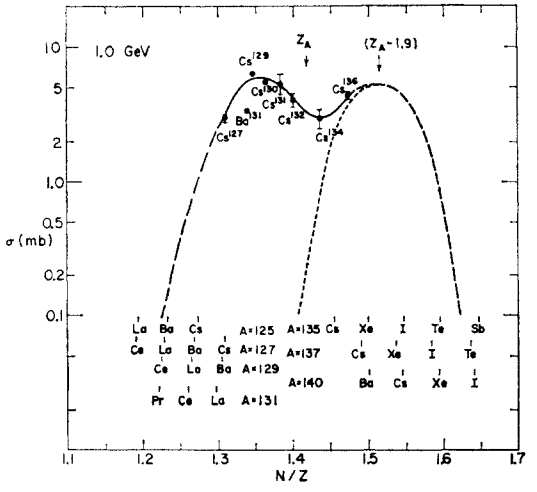

FIG. 15. Charge dispersion at 1.0 GeV. The dashed wings of the curve have been drawn so that the sums of the isobaric yields read off the curve approximate the *measured* cumulative yields:

	Experimental σ (mb)	Curve σ (mb)
Cs^{136}	1.1	1.1
Ba^{127}	1.4	1.2
Ba^{129}	3.6	3.6
La^{131}	2.4	3.0
Cs^{135}	13	13.3
Cs^{137}	9.6	11.0
Ba^{140}	9.3	10.1

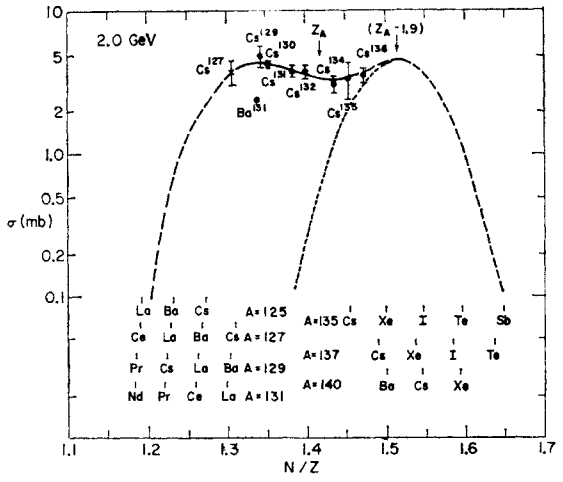

FIG. 16. Charge dispersion at 2.0 GeV. The dashed wings of the curve have been drawn so that the sums of the isobaric yields read off the curve approximate the *measured* cumulative yields:

	Experimental σ (mb)	Curve σ (mb)
Cs^{125}	2.7	3.0
Cs^{127}	7.2	6.4
Ba^{129}	5.4	6.0
La^{131}	4.4	5.5
Cs^{135}	14.7	13.0
Cs^{137}	10.8	10.3
Ba^{140}	8	9.6

The value for Cs^{127} shown on the graph as a cross is interpolated from the excitation function as described in the caption of Fig. 7. The "experimental" value shown above for Ba^{140} is interpolated from the excitation function.

The important general features of the charge-dispersion curves may be summarized as follows: As the bombarding energy is increased from 0.10 to 0.38 GeV, the curves become broader and the peak position moves to smaller N/Z ratios. In Table VI are given the full width at half-maximum and peak positions for these energies.

The N/Z value at the peak, together with the mass number of the cesium isotope nearest the peak, was used to obtain Z_P, the most probable fragment charge for this mass. The difference between Z_A and Z_P for this mass is given in the table. The N/Z values at half-maximum were similarly converted to Z values for this same mass to obtain full width at half-maximum values in Z units. The values in Table VI, together with data of Aagard *et al.*[24] for U fission by 0.17-GeV protons and data of Pate *et al.*[25] for Th fission by protons of up to 0.087 GeV, are shown in Figs. 19 and 20.

At higher energies, 0.68 to 2.9 GeV, the curves begin to show structure with a valley appearing near the region of β stability. As with the lower energy data, the cumulative yields (now both on the neutron-deficient and neutron-excess sides) define the shapes of the curves within narrow limits. At 0.68 GeV (Fig. 14), structure is discernible although not very pronounced; at the higher energies it is not possible to draw the distribution curves without a double peak. It is interesting to note that once the peak on the neutron-excess side becomes clearly discernible, the peak position appears to remain virtually unaltered with increasing energy at an N/Z value of 1.515. If one assumes this peak to be symmetrical and obtains its left wing by reflection of the right-hand portion around the peak position, one finds a half-width of about 0.11 N/Z unit, corresponding to 2.5 Z units for a given A. Both the peak position and the half-width thus correspond to fission by protons of about 50-MeV bombarding energy, as indicated by comparison with the curves in Figs. 19 and 20. Indeed, the broadening and shift of the curves at lower energies may already indicate the incipient structure with the two peaks as yet unresolved. It is, for example, possible to construct two separate symmetrical curves with peaks at N/Z values of 1.41 and 1.52 which add to the broad single-humped curve observed at 0.38 GeV (Fig. 13). This may well account for the fact that, as shown in Fig. 19,

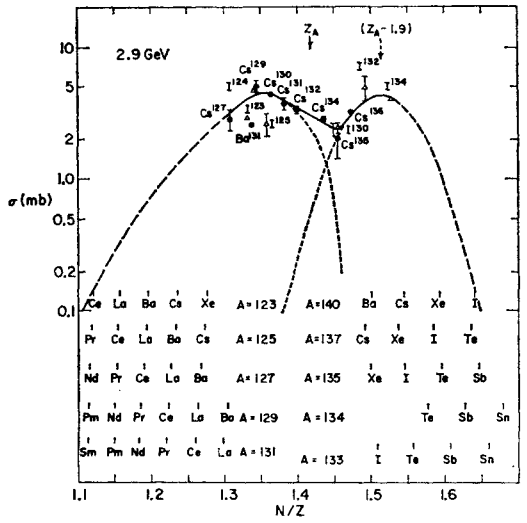

FIG. 17. Charge dispersion at 2.9 GeV. Data from the paper by Alexander *et al.* (reference 16) are included (triangles) to show that the assumption of a flat mass-yield curve in the region under discussion is justified. The dashed wings of the curve have been drawn so that the sums of the isobaric yields read off the curve approximate the *measured* cumulative yields:

		Experimental σ (mb)	Curve σ (mb)
I^{123}	(reference 16)	8.9	8.6
Cs^{125}		3.9	4.5
Ba^{127}		4.7	4.2
Ba^{129}		6.7	6.9
La^{131}		6.0	6.5
I^{133}	(reference 16)	9.2	8.0
Te^{134}	(reference 16)	3.7	2.3
Xe^{135}		10.0	8.7
I^{135}	(reference 16)	4.8	4.6
Cs^{137}		8.8	9.5
Ba^{140}		7.9	9.0

The analysis of the curve into two components (dotted portions) is discussed in the text.

[24] P. Aagard, G. Andersson, J. O. Burgman, and A. C. Pappas, J. Inorg. Nucl. Chem. **5**, 105 (1957).

[25] B. D. Pate, J. S. Foster, and L. Yaffe, Can. J. Chem. **36**, 1691 (1958).

the width of the 0.38-GeV distribution is larger than one might expect by extrapolation of the lower energy results.

With increasing energy, the neutron-deficient peak becomes more prominent, shifts slightly to lower N/Z values, and becomes wider.

From the charge-dispersion curves at various bombarding energies, it is now possible to deduce the total fission yield per mass number in the region of $125<A<140$ as a function of energy. These yields were obtained by summing the individual independent yields of all the isobars of any one mass as obtained from these curves. The total fission yield per mass number in this region (actually for $A=131$) is plotted against bombarding energy in Fig. 21. It is seen to decrease from about 52 mb at 0.1 GeV to about 29 mb at 1.0 GeV and then to remain essentially constant. That portion of the isobaric yield associated with the neutron-excess peak was obtained separately at each of the three highest energies (under the assumptions that these peaks are symmetrical), and this contribution is about 12 mb at 1, 2, and 3 GeV (Fig. 21).

The independent yields obtained for Ba^{131} (measured as Cs^{131}) fall consistently below the charge-dispersion curves (see especially Figs. 13–17). One possible reason for this result could be the existence of an isomer of Ba^{131}, either decaying directly to Cs^{131} or decaying to 11.5-day Ba^{131} with a half-life long compared to 11.5 days. Some credence is lent to this hypothesis by the existence[5] of isomeric states in the other odd-A Ba isotopes ($Ba^{129,133,135,137}$).

Note added in proof. As a result of the above considerations, a search for an isomer of Ba^{131} was initiated, and such an isomer, with half-life of 14.6 min, was indeed identified by R. S. Tilbury and L. Yaffe [Phys. Rev. **129**, 1709 (1963)]. However, these authors have shown that this isomer decays entirely by isomeric transition to the 11.5-day ground state of Ba^{131}. Its existence thus does not explain the cross section anomaly for Ba^{131} observed in the present work since any 14.6-min Ba^{131m} formed would, in our experiments, have appeared together with 11.5-day Ba^{131}.

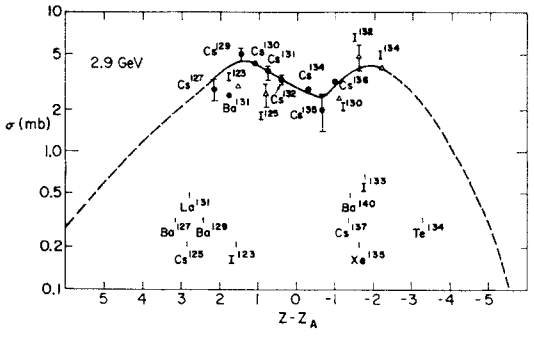

FIG. 18. Charge dispersion at 2.9 GeV, drawn with $(Z-Z_A)$ as the abscissa. The $(Z-Z_A)$ values given for the nuclides whose cumulative yields were used in defining the wings of the curve are those appropriate (reference 23) for $N<82$.

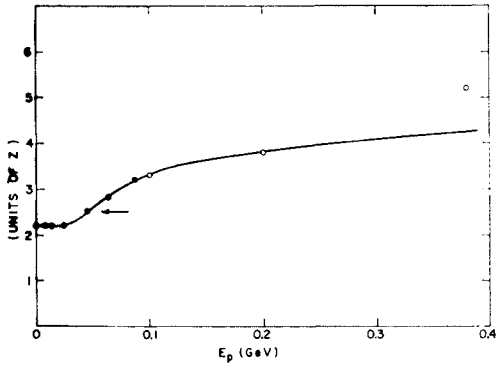

FIG. 19. Width of charge dispersion as a function of bombarding energy. The full width at half-maximum is given in units of Z. The solid points are taken from reference 25, the open circles from the present work. The width of the neutron-excess peak observed at 1–3 GeV is indicated by the arrow.

IV. DISCUSSION

In this section will be given a qualitative discussion of the experimental data reported. More quantitative interpretation, in terms of actual reaction mechanisms, must await further theoretical calculations of high-energy nuclear interactions.

It is clear from the charge-dispersion curves in the GeV region and the recoil data given in Table III that low-deposition-energy processes still contribute significantly to the fission cross section at these energies. This is evidenced by the position and width of the neutron-excess peaks in the charge-dispersion curves, which, as shown in Figs. 19 and 20, correspond to the characteristics of fission induced by protons of approximately 50-MeV bombarding energy. The fact that the ratio of forward-to-backward recoil losses of Ba^{140} (Table III) remains close to unity also indicates clearly a low-deposition-energy mechanism for the formation of this nuclide. Additional recoil experiments attesting to this mechanism are presented by Alexander *et al.*[16] The integrated yield per mass number for the low-deposition-energy fission process is $\sim$12 mb from 1 to 3 GeV (Fig. 21). Based on the mass-yield distribution and total cross section for fission by 50-MeV protons,[22] one deduces a cross section of approximately 500 mb for this low-deposition-energy process at GeV energies. This is considerably higher than the cross section for such low-deposition-energy processes predicted by the Monte Carlo calculations of nuclear cascades by Metropolis *et al.*[26]

From consideration of the charge-dispersion curves and the recoil behavior of Ba^{131} (Table III), it is apparent that the neutron-deficient nuclides arise from high-deposition-energy processes. The decrease in the fractional loss of Ba^{131} as the incident proton energy increases from 0.38 to 2.9 GeV (shown in column 5 of Table III) would indicate a decrease in the kinetic

[26] N. Metropolis, R. Bivins, M. Storm, J. M. Miller, G. Friedlander, and A. Turkevich, Phys. Rev. **110**, 204 (1958).

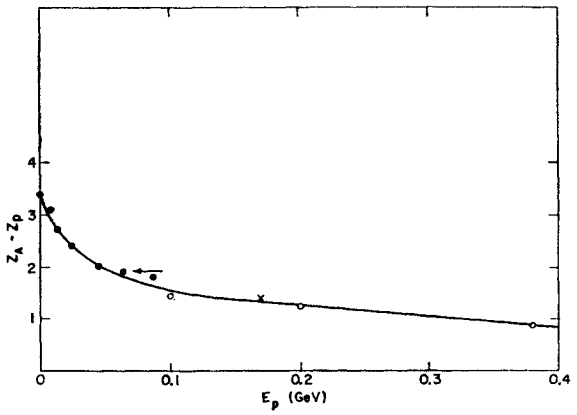

FIG. 20. Plot of Z_A-Z_p as a function of bombarding energy. Solid points are from reference 25, the point at 0.17 GeV (cross) from reference 24, the open circles are from the present work. The position of the neutron-excess peak observed at 1–3 GeV is indicated by the arrow.

energy of Ba^{131}. This can be accounted for by a fission partner of lower mass at the higher energies and, therefore, a *lighter* fissioning parent and is, in turn, consistent with greater energy deposition in the initial interaction reflected by the large forward-to-backward recoil ratio. As Alexander *et al.*[16] point out, processes other than binary fission may well be important contributors to the formation of highly neutron-deficient products in this mass range.

The increasing contribution of neutron-deficient products to the total fission cross section, with increasing bombarding energy, is in a qualitative way readily accounted for in terms of increasing energy deposition leading to increasing neutron evaporation either prior to or after fission. On this basis, one might expect the charge-dispersion curves to become lower and broader with increasing bombarding energy, extending further and further to the neutron-deficient region. The surprising feature of the present data is the appearance of the valley in these curves. The existing Monte Carlo cascade calculations[26] do not show a corresponding deficiency of intermediate excitation energies. This, however, may be the result of the already mentioned underestimation of low deposition energies inherent in these calculations. Other possible explanations may lie in some feature of the fission-evaporation competition as a function of excitation energy and Z^2/A. Dostrovsky *et al.*[27] have pointed out that whether or not the evaporation path from a given initial nuclide will lead to a Z^2/A value favorable for fission may depend critically on the initial excitation energy. At low initial excitations, only neutrons tend to be evaporated, leading to ever-increasing Z^2/A values; at higher excitation, charged-particle (especially alpha) emission becomes probable early in the evaporation chain, with a corresponding decrease in Z^2/A; but at still higher initial excitations, the evaporation path, after some charged-particle evaporation, may again lead to larger Z^2/A values.

Additional information about the mechanism can be deduced from the energies of the excitation function maxima. The data in Fig. 9 would indicate that the very neutron-deficient cesium isotopes $Cs^{125-127}$ and the rubidium isotopes straddling the stability line (Rb^{84} and Rb^{86}) are formed in similar processes. The postulate of equal charge displacement[28] is, thus, very unlikely to be operative in the formation of these products. On the other hand, the correlation of excitation function shapes with N/Z ratios speaks for fission with unchanged charge distribution (UCD).[29] At first sight, the most attractive hypothesis would appear to be UCD fission with very little or no post-fission evaporation. For a product such as Rb^{86}, the fissioning parent would then have to be as neutron deficient as Pa^{212} or Th^{210}. The formation of such neutron-poor products in appreciable yield is completely at variance with evaporation calculations.[30] One must therefore turn to the alternative of fission from a fairly high state of excitation, followed by some post-fission evaporation. The question then arises why different end products of such a process should have the same or very similar neutron-proton ratios, except by pure coincidence in particular cases.

Consider[31] a fissioning nucleus of mass number A_0, atomic number Z_0, and excitation energy E_0 and suppose it fissions according to the UCD postulate and with the excitation energy being divided among the products proportional to their masses. If one of the primary fission fragments is characterized by A_1, Z_1, E_1, it

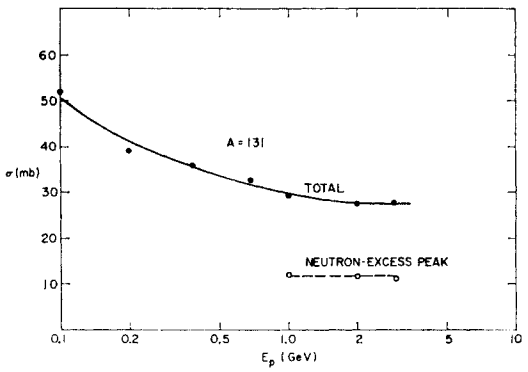

FIG. 21. Total isobaric cross section for $A = 131$ obtained from the charge-dispersion curves. The contribution from the neutron-excess peak at 1 to 3 GeV is shown separately.

[27] I. Dostrovsky, Z. Fraenkel, and P. Rabinowitz, *Proceedings of the Second United Nations International Conference on the Peaceful Uses of Atomic Energy, Geneva, 1958* (United Nations, Geneva, 1958), Vol. 15, p. 301.

[28] L. Glendenin, C. D. Coryell, and R. R. Edwards, Phys. Rev. **75**, 337 (1949); and L. Glendenin, Ph.D. thesis, Massachusetts Institute of Technology, 1949 (unpublished).

[29] R. H. Goeckerman and I. Perlman, Phys. Rev. **76**, 628 (1949).

[30] I. Dostrovsky, P. Rabinowitz, and R. Bivins, Phys. Rev. **111**, 1659 (1958).

[31] The considerations in this paragraph were developed as a result of a suggestion by Professor J. M. Miller, whose contribution is hereby most gratefully acknowledged.

follows that $A_1/Z_1=A_0/Z_0$ and $E_1/Z_1=E_0/Z_0$. Assume now for simplicity that only neutrons are evaporated and that the amount of energy lost per evaporated neutron is a constant, ΔE. The final product will then have mass number $A_2=A_1-(E_1/\Delta E)$, and its mass/charge ratio will be given by

$$\frac{A_2}{Z_1}=\frac{A_1-E_1/\Delta E}{Z_1}=\frac{A_0-E_0/\Delta E}{Z_0}.$$

The neutron-proton ratio of the final product is, thus, under the simplifying assumptions made, completely determined by the characteristics of the fissioning nucleus and by the constant ΔE. The use of a constant ΔE, independent of excitation and of A and Z, is a very reasonable approximation over a fairly wide range of A, Z, and E.[30] The inclusion of proton evaporation does not appear to change the results drastically. Suppose the primary fragment (A_1, Z_1, E_1) is de-excited to the final product (A_2, Z_2) by evaporation of neutrons and protons, with the fraction f of the excitation E_1 being dissipated by proton emission, the remainder by neutron emission. Let ΔE_p be the average de-excitation per emitted proton; ΔE is now the average de-excitation per nucleon. Then

$$\frac{A_2}{Z_2}=\frac{A_1-E_1/\Delta E}{Z_1-fE_1/\Delta E_p}=\frac{A_0-E_0/\Delta E}{Z_0-E_0(f/\Delta E_p)}.$$

According to the calculations of Dostrovsky *et al.*,[30] $(f/\Delta E_p)$ is of the order of 0.01 or less, and the denominator is therefore not expected to differ from Z_0 by more than a few percent; furthermore, in the comparison of A_2/Z_2 ratios of different end products, only the *differences* between values of $(f/\Delta E_p)$ enter. Thus, it becomes entirely reasonable that the excitation function maxima should be correlated with the A/Z (or N/Z) ratios of the products, provided UCD fission anywhere along the evaporation path is assumed and excitation energy is distributed among the primary fragments according to their masses. It would still be of interest to determine whether the curve in Fig. 9(a), in fact, represents a universal function over a wide range of Z and A.

ACKNOWLEDGMENTS

The authors acknowledge gratefully assistance from the following: Dr. R. W. Stoenner, Dr. K. Rowley, and Miss E. Norton who performed numerous chemical analyses; the operating staffs at the Nevis Cyclotron and Brookhaven Cosmotron; Dr. J. M. Miller, Dr. N. Sugarman, and Dr. J. Alexander who kindly arranged the irradiations at the Nevis, Chicago, and Berkeley accelerators, respectively; Dr. L. P. Remsberg and Dr. K. Rind who were particularly helpful in the experiments carried out at the Nevis Cyclotron; Miss E. M. Franz who ably assisted in some of the experiments; and F. Silkworth who cheerfully prepared many of the high-purity reagents used in the mass-spectrometric studies. Helpful and stimulating discussions with Dr. J. M. Miller and Dr. J. Alexander are acknowledged with particular pleasure.